

Supplemental Data

to Al-Samir et al.: Activity and distribution of intracellular carbonic anhydrase II and their effects on the transport activity of anion exchanger AE1/SLC4A1

Figure S1

murine AE1 C-terminus

894 L I F R E L E L Q C L D G D D A K V T F D E E N G L D Y E D E V P M P V

human AE1 C-terminus

876 L I F R N V E L Q C L D A D D A K A T F D E E E G R D Y E D E V A M P V

wt CAII N-terminus

M¹ S H H W G Y G K H N G P E H W H K D F P I A K G E R Q S P —

truncCAII N-terminus

M¹ G E R Q S P —

Fig. S1. Proposed interacting regions of AE1 and CAII. Upper part: the C terminus of mAE1 and hAE1 possess a motif (labelled in yellow) of 5 amino acids, containing one L and three D, proposed to mediate binding to CAII. Lower part: the N terminal region of CAII, containing 5 histidines and 1 lysine (labelled in yellow) suggested as participating in binding to the C terminal tail of AE1. The lowest line shows the site of N-terminal truncation of construct “truncCAII”, with deletion of the amino acids proposed to participate in AE1 binding.

Figure S2

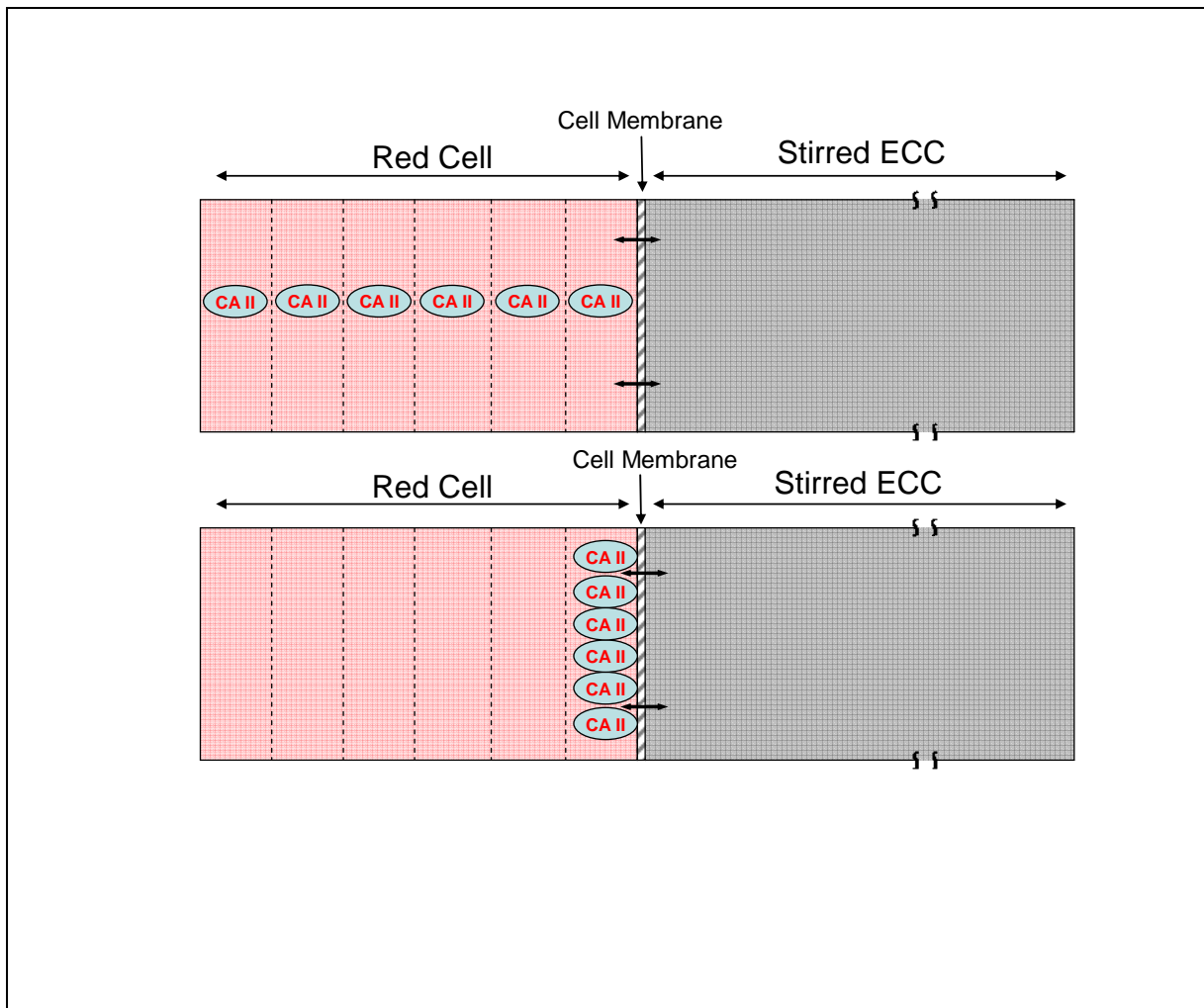


Fig. S2. Scheme explaining the theoretical model used to simulate HCO_3^- and CO_2 transport across a cell membrane. The calculations were performed for the parameters of a human red cell. The extracellular compartment was considered to be well-stirred. The intracellular compartment was divided into 80 segments per red cell half-thickness, and a finite difference method was used to solve the system of differential equations describing diffusion of CO_2 and HCO_3^- as well as buffer-facilitated H^+ diffusion. In conjunction with these diffusion processes the simultaneous reactions $\text{CO}_2 + \text{H}_2\text{O} \leftrightarrow \text{HCO}_3^- + \text{H}^+$ and $\text{H}^+ + \text{Hb} \leftrightarrow \text{HbH}^+$ were considered. The results of the calculations are shown in Figs. 8 and 9. In the upper scheme a cytoplasmic carbonic anhydrase activity of 20,000 (activity defined as acceleration factor of CO_2 hydration minus 1) was assumed to be present everywhere inside the cell. To study the effect of complete binding of all intraerythrocytic CA at the internal side of the membrane (lower scheme of Fig. 1), the total amount of CA present in the red cell was assumed to be accumulated in the last segment immediately adjacent to the cell membrane (segment thickness $0.01 \mu\text{m}$, CA activity in this segment, $80 \times 20,000$).

Figure S3

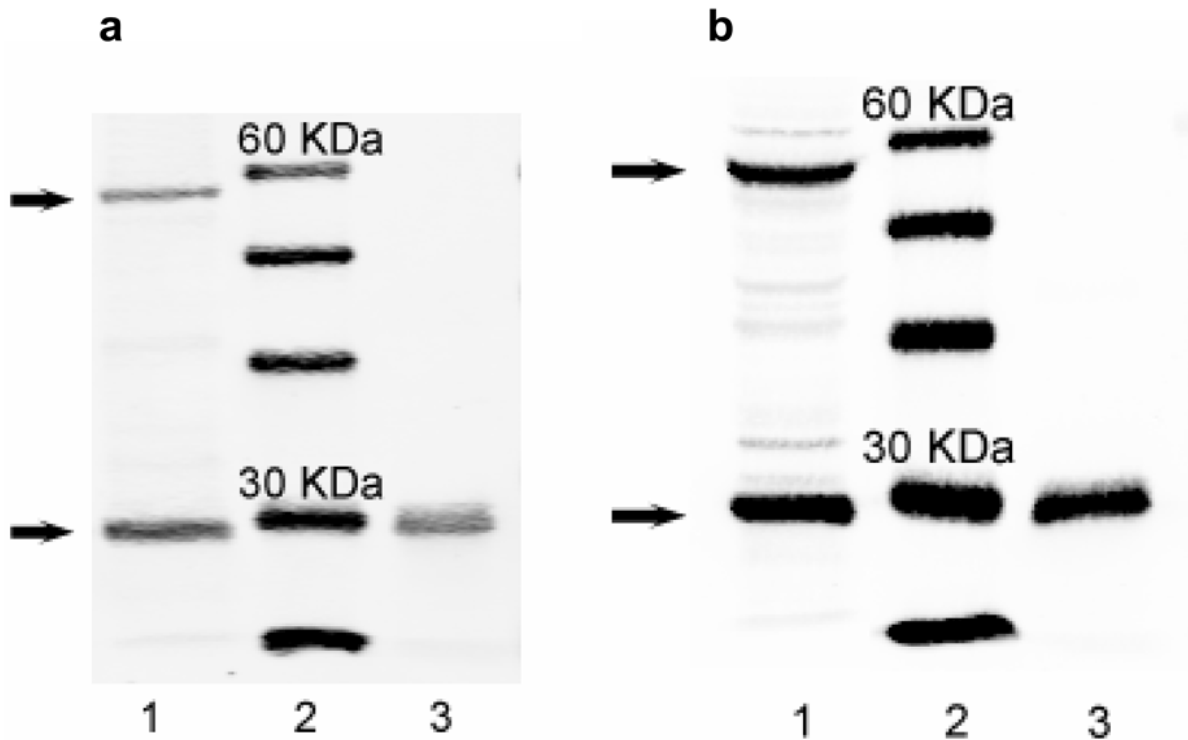


Fig. S3. Western Blots showing expression of fluorescent CAII fusion proteins in tsA201 cells. a) Lane 1: upper band is WT-CAII-CyPet, lower band is endogenous CAII of tsA201 cells. Loaded lysate derived from $\sim 1 \times 10^5$ cells (corresponds to 7 μg protein) ; Lane 3: CAII of human red cell lysate. b) Lane 1: upper band is non-catalytic mutant CAII-V143Y-CyPet, and lower band is endogenous CAII of tsA201 cells. Loaded lysate derived from $\sim 1.4 \times 10^6$ cells (corresponds to 99 μg protein), transfection efficiency was 25% in this case, i.e. unusually low. Lane 3: CAII from human red cell lysate. Western Blotting was done similarly to the procedure described by IteI et al. (2012). Cells were harvested 3 days after seeding. Primary rabbit anti-CAII antibody (Acris Antibodies) was applied over night at 4°C, diluted 1:5000 in PBS -Tween. Binding of the antibody was detected using the Li-Cor Odyssey Infrared Imaging System.

Figure S4

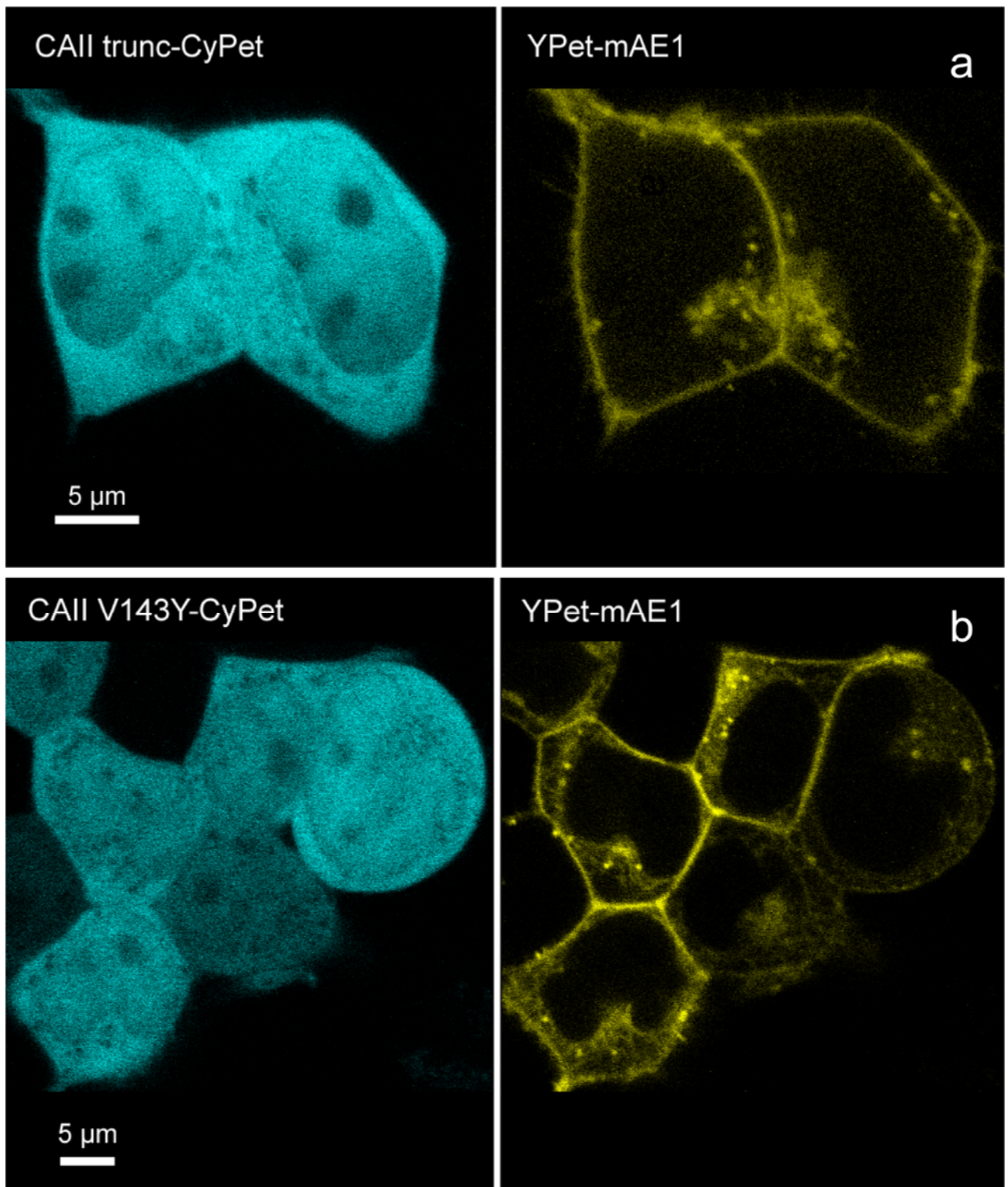


Fig. S4. a) Confocal microscopic images of tsA201 cells co-transfected with N-terminally truncated CA II-CyPet (left) and YPet-mAE1 (right). Intracellular distribution patterns are identical to those in Fig. 2. b) tsA201 cells co-transfected with non-catalytic CAII mutant CAII-V143Y-CyPet (left) and YPet-mAE1 (right). Distribution patterns are identical to those in Fig. 2.